Supplementary Information

Collaboratively boosting charge transfer and CO_2 chemisorption of SnO_2 to selectively reduce CO_2 to HCOOH

Yusheng Yuan, Kai Sheng, Guilin Zhuang, Qiuyan Li, Cong Dou, Qiao-jun Fang, Wen-wen Zhan,* Hao Gao, Di Sun* and Xiguang Han*

1. Experimental detail

1.1 Synthesis of Sn-MOF precursor. $SnSO_4$ (0.105 g, 0.49 mmol) and terephthalic acid (0.12 g, 0.72 mmol) were mixed in the glass vial following by adding 6 mL DMF. Then, the mixture was transferred to a 25 mL Teflon-lined stainless steel autoclave and heated at 180 °C for 20 h. After slowly cooled to room temperature, colorless block shaped crystals were isolated by decanting the supernatant liquid and washed thoroughly with ethanol.

1.2 Synthesis of SnO_2-V_O@N-C porous rods. SnO_2-V_O@N-C PR were synthesized via calcination of the obtained Sn-MOFs precursor at 600 °C for 180 min in Ar atmosphere with heating rate of 2 °C·min^{-1}.

1.3 Synthesis of pure SnO_2 porous rods. Pure SnO_2 were synthesized via calcination of the obtained SnO_2-V_O@N-C PR at 600 °C for 200 min in O_2 atmosphere with heating rate of 2 °C·min^{-1}.

1.4 Synthesis of SnO_2-V_O porous rods. SnO_2-V_O porous rods were synthesized via the thermal treatment of Pure SnO_2 at 600 °C for 200 min under the vacuum atmosphere.

1.5 Characterization

1

The composition and phase of the as-prepared products were acquired by the powder X-ray diffraction (XRD) pattern using a Panalytical X-pert diffractometer with CuKα radiation. The morphology and crystal structure of as-prepared products were observed by scanning electron microscopy (SEM, SU8100), and high-resolution transmission electron microscopy (HRTEM, FEI Tecnai-F20) with an acceleration voltage of 200 kV. All TEM samples were prepared from depositing a drop of diluted suspensions in ethanol on a carbon film coated copper grid. PHI QUANTUM2000 photoelectron spectrometer (XPS) was using to characterize the surface compositions of product. The surface areas of these samples were measured by the Brunauer-Emmett-Teller (BET) method using nitrogen adsorption and desorption isotherms on a Micrometrics ASAP 2020 system. The element contents of C, N, and H in the sample were measured by Elementar Analyzer of Vario EL III.

1.6 Electrocatalytic reduction of CO_2

6 mg of sample was dispersed in 0.5 mL of mixed solvent containing Nafion solution (5 wt%, 70 μL), H_2O (350 μL), and ethanol (80 μL) to form a homogeneous ink after at least 60 min ultrasonic treatment. Then 84 μL of the catalyst ink was loaded onto a carbon paper (1 cm^2), The catalyst loading was $\approx$ 1 mg·cm^{-2}, and considering that SnO_2 is the mainly active sites, the amount of catalyst responsible for the reduction of CO_2 can be determined as about 0.78 mg·cm^{-2}, Then, the electrodes were dried at 60 °C for 2 h before testing.

Electrochemical CO_2 reduction was performed in a gastight two-compartment electrochemical cell separated by a Nafion 117 membrane with a three-electrode setup, Pt mesh and SCE were used as the counter and reference electrodes. The reference electrode potentials were converted to RHE using the formula below, and the measured potentials (vs SCE) were converted to RHE using the formula E(RHE) = E(SCE) + 0.241 V + 0.0591 $\times$ pH. The electrolyte was 0.1 M potassium bicarbonate ($KHCO_3$, $\geqslant$99.95%) saturated with CO_2 (pH = 6.8). Before electrolysis, the electrolyte was purged with CO_2 gas (99.999%) for at least 30 min.

Each compartment contained 35 mL of electrolyte with a 20 mL headspace. The electrolyte in the cathodic compartment was stirred at a rate of 600 rpm to enhance mass transport of CO_2 and products around the surface of the working electrode. The CO_2 reduction was performed for 1 h at various potentials in the electrolyte. The electrochemical measurements were carried out using a potentiostat (CHI-760E). The current densities reported in this work were normalized to the geometric surface area. The electrochemical surface areas (ECSAs) was calculated according to the equation: $ECSAs = R_f S$, where R_f represented the roughness factor of the SnO_2-based electrocatalyst and S represented the real surface area of working electrodes (S = 1 cm^2). R_f was estimated according to the relation $R_f = C_{dl}/C_{dlref}$ based on the Cdl of a smooth oxide surface (60 $\mu F/cm^2$ for C_{dlref} of SnO_2). The CO_2 electroreduction test was repeated three times and the results presented are the averaged values. All the experiments were conducted under ambient pressure and at room temperature (25 °C).

CO_2RR Products Analysis: A gas chromatograph (GC9790Ⅱ, Fuli) with a thermal conductivity detector and a flame ionization detector was used to quantify the concentration of gaseous products including H_2 and CO. The concentration of reaction products in the liquid electrolyte was detected using a 500 MHz 1H liquid NMR spectrometer (Bruker Advance) with the water suppression method. N,N-dimethylformamide was used as an internal reference for the chemical shifts. Typically, NMR samples were prepared by mixing 100 μL of the product-containing electrolyte, 1 μL of N,N -dimethylformamide (≥99.9%,) and 599 μL D_2O (99.9%). Formate calibration curves (Figure S3) were generated using a stock solution of sodium formate. Assuming that two electrons are needed to produce one formate molecule, the FE can be calculated as follows: FE = 2F × nformate/Q = 2F × n formate/(I × t), where F is the Faraday constant.

1.7 Density Functional Calculations

All of the density functional theory (DFT) calculations were performed by using Vienna ab-

initio Simulation Package (VASP). [1] The exchange-correlation energy was described with the generalized gradient approximation (GGA) and the Perdew-Burke-Ernzerhof (PBE). [2] Core electrons effect on the valence electron density were treated by using Projector Augmented Wave (PAW) method [3]. The cutoff energy for the plane wave basis sets was 400 eV. The convergence threshold of atoms position and cell parameters were set to be 10^{-5} eV in energy and 10^{-2} eV/Å in force. The DFT-D3 method was used to describe the van der Waals (vdW) interactions between different reaction molecules. [4] The Brillouin zone was sampled by k-points mesh of 1´1´1.

The Gibbs free energy calculation followed the work of Nørskov et al. [5] Under the standard reaction condition, the chemical potential of a proton and electron pair (μ ($H^+ + e^-$)) is equal to a half of gaseous hydrogen (μ (H_2)). For each elemental step, the Gibbs free energies (DG) was calculated by following equation:

$$\Delta G = \Delta E_{DFT} + \Delta ZPE + \Delta H - T\Delta S + \Delta G_{pH}$$

(1)

where E is the total energy calculated by VASP, ZPE is the zero point energy, H, S are the heat capacity and entropy, T is equal to 298 K. G_{pH} is the influence caused by pH value.

Where n is the transferred electron number.

$$G_{pH} = -k_B T ln(H^+) = pH \times k_B T ln 10$$

(2)

where k_B is the Boltzmann constant. All calculation presented here, pH is typically set as zero.

The adsorption energies (E_{ads}) of the different adsorbates was calculated by the expression:

$$E_{ads} = E_{total} - (E_{catal} + E_{mol})$$

(3)

where E_{total} shows the total energy of slab after adsorption, E_{catal} is the energies of bare catalyst, and the E_{mol} denotes the total energies of an adsorbate molecule including the CO_2, COOH, HCOOH, CO.

2. Experimental results

Figure S1 (a) The XRD pattern of Sn-MOF precursor. (b) FE-SEM images of Sn-MOF precursor.
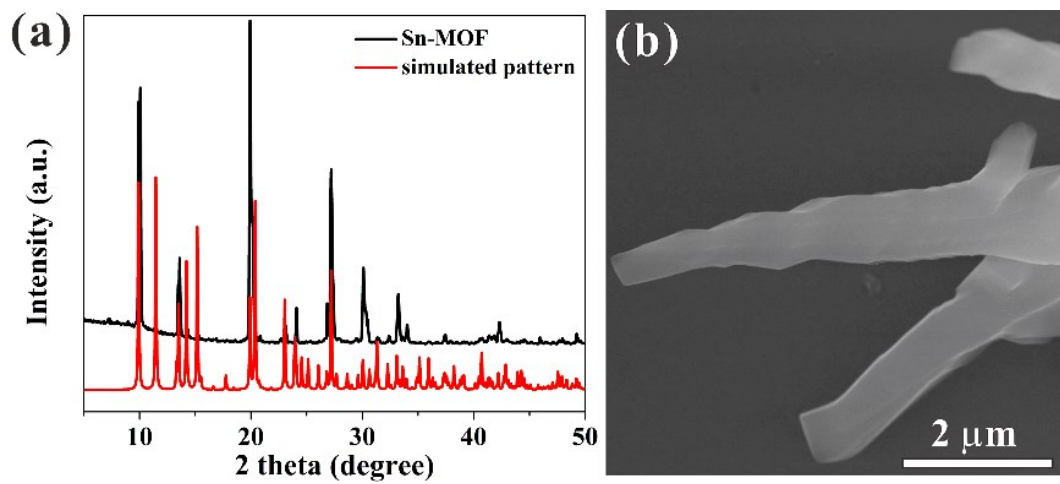
Figure S2 (a) SEM image of Sn-MOF precursor, (b-f) Element mapping of Sn-MOF precursor.
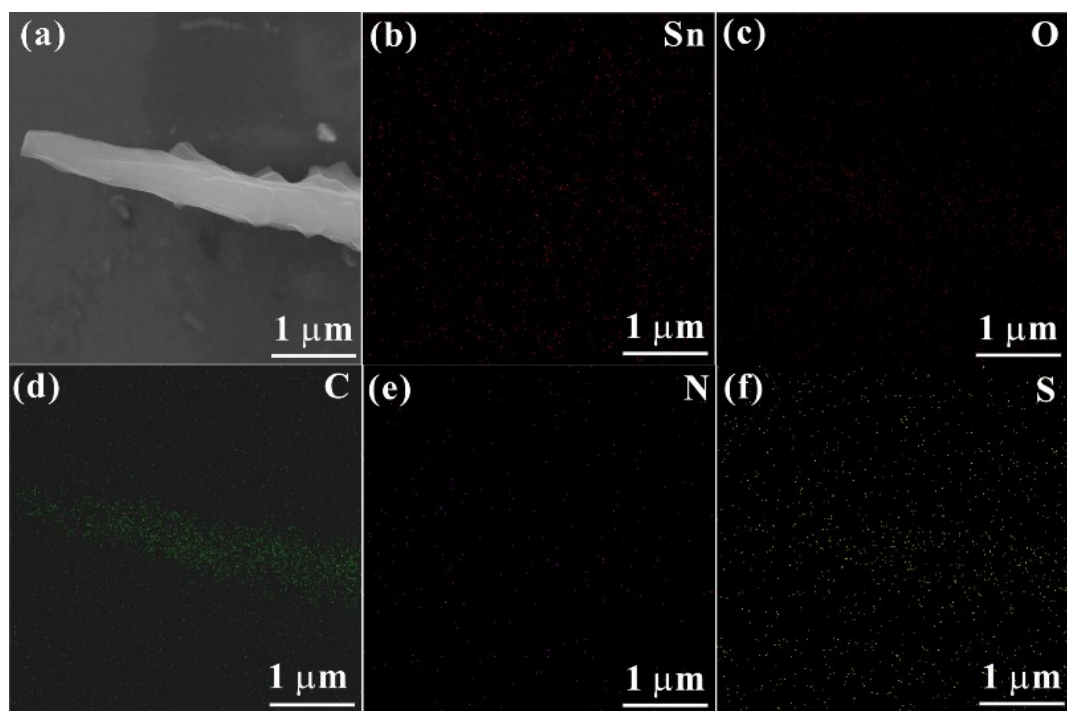
Figure S3 TGA of Sn-MOF precursor.
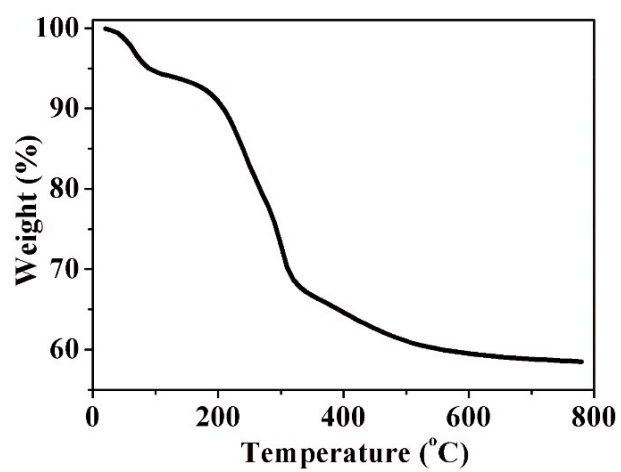
Figure S4 N_2 adsorption/desorption isotherms of SnO_2-V_O@N-C PR.
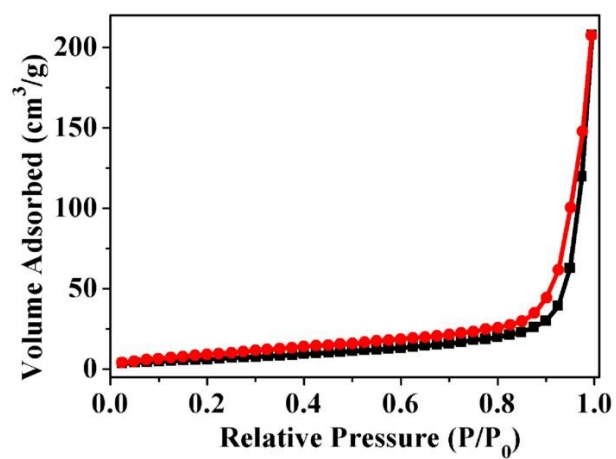
Table S1. Mass content and atomic content of the various elements in SnO_2-V_O@N-C.

Element	N	C	H	Sn	O
Mass content (%)	0.327	10.37	0.553	61.70	26.90
Atomic content (%)	0.6	23.7	15.2	14.3	46.2

The mass contents of C, N, and H in SnO_2-V_O@N-C were firstly measured by Elementar Analyzer of Vario EL III. Then combined with the XPS result of O 1s, the mass content of Sn and O was calculated as 61.70% and 26.90%. Finally, the atomic contents of these elements were calculated and listed in the above Table.

Figure S5 (a) The XPS survey spectrum of SnO_2-V_O@N-C PR. (b) The high-resolution O 1s spectrum of SnO_2-V_O@N-C PR.
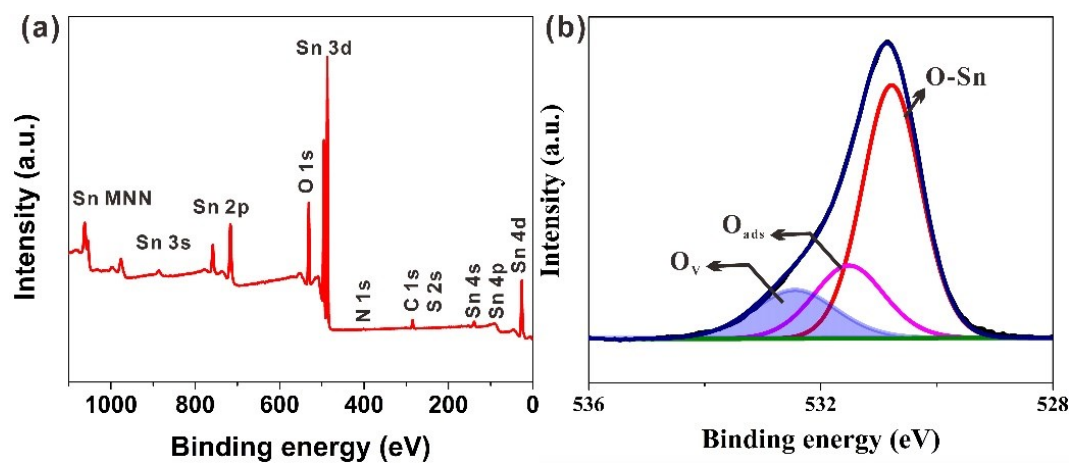
Figure S6 (a) The XRD pattern of pure SnO_2 PR. (b) The typical SEM image of pure SnO_2 PR.

(c) and (d) The corresponding elemental mapping profiles.
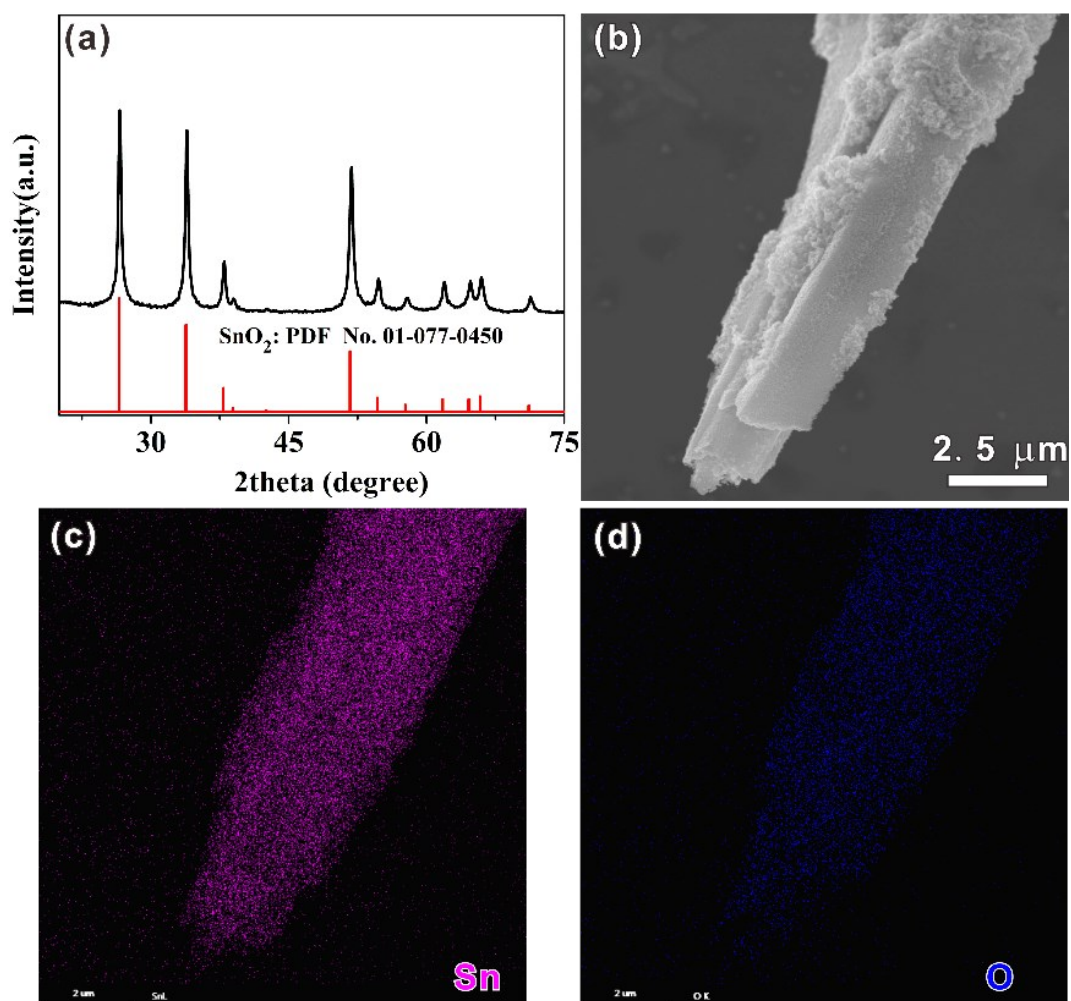
Figure S7 The high-resolution O 1s spectrum of pure SnO_2 PR.
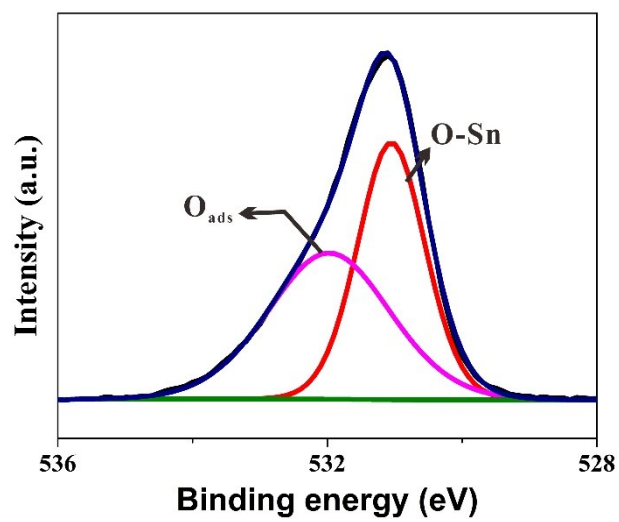
Figure S8 (a) LSV curves, (b) partial current density for HCOOH, and (c) FE of HCOOH over

SnO_2-V_O@N-C with different concentration of $KHCO_3$ as the electrolyte.
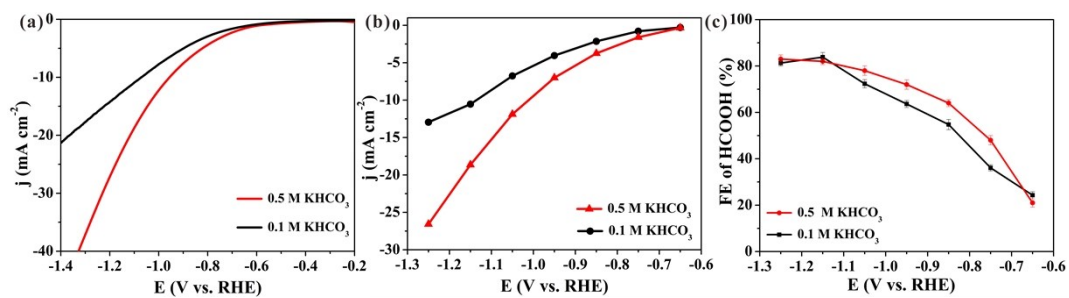
Figure S9 LSV curves of SnO_2-V_O@N-C in CO_2-saturated solution (red line) and N_2-saturated solution (black line) and blank experiment (black carbon, blue line).
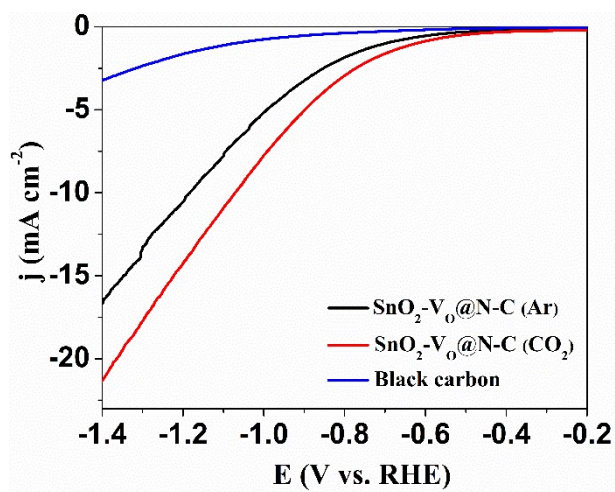
Figure S10 (a) EPR spectra of SnO_2-V_O@N-C, SnO_2-V_O and pure SnO_2. (b) The high-resolution O 1s spectrum of SnO_2-V_O PR.
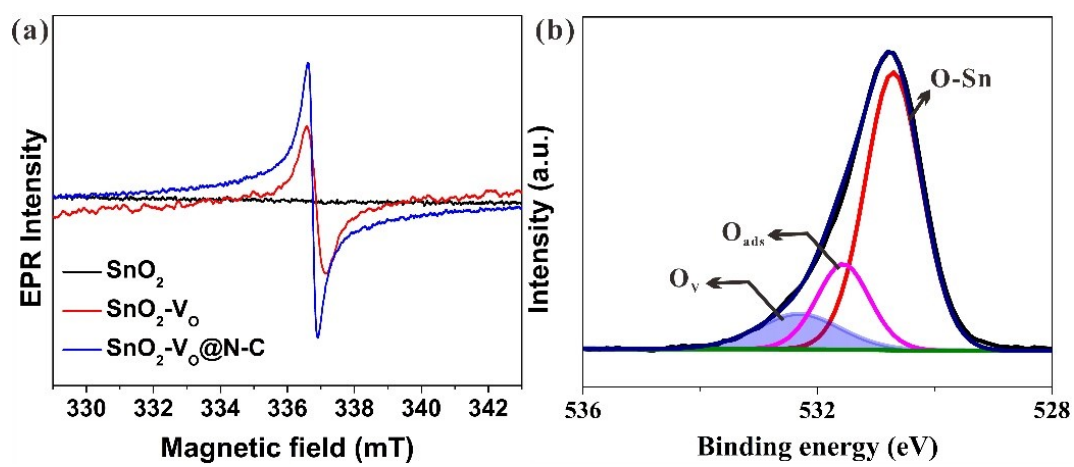
Figure S11 Gas chromatograph identification of standard gas with (a) TCD and (b) FID.
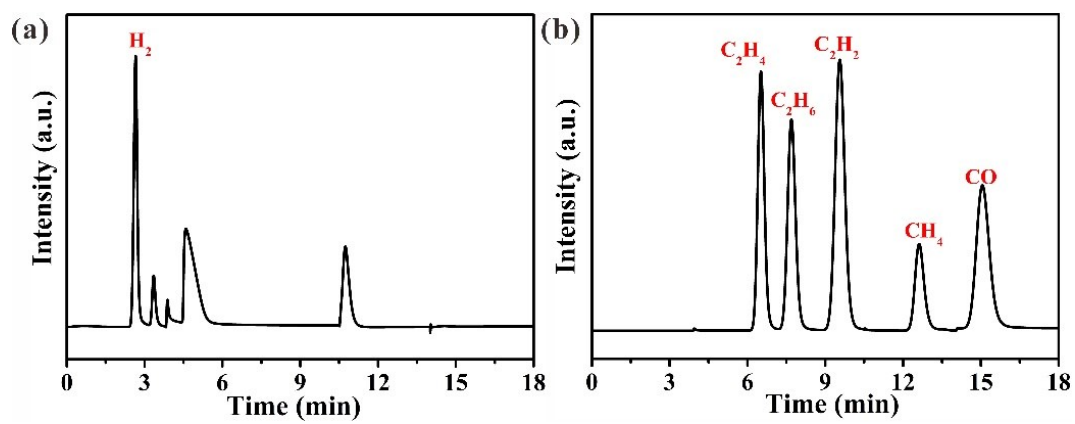
Figure S12 Gas chromatograph identification of H_2 and CO production for CO_2 reduction reaction over SnO_2-V_O@N-C.
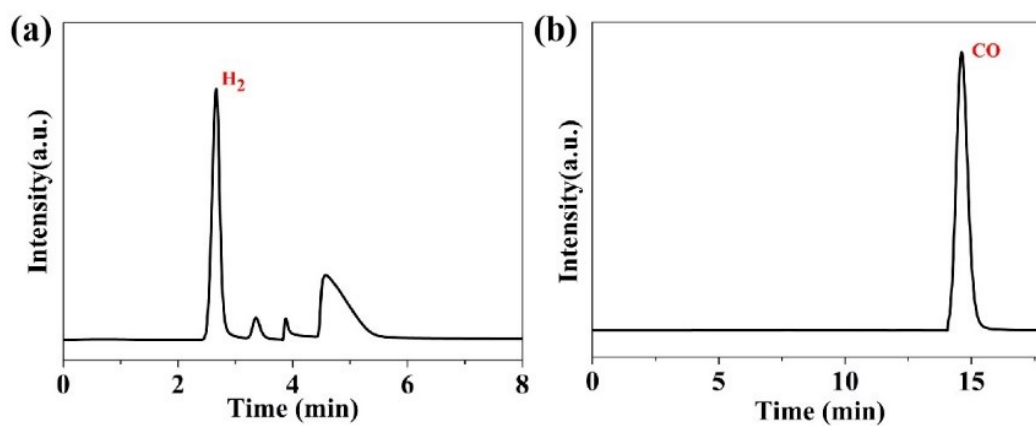
Figure S13 (a) Linear relationship between the formate concentration and relative peak area vs. DMF. (b) NMR spectrum of 0.1 MKHCO; electrolyte after 1 h of CO$_2$RR at -1.15 V.
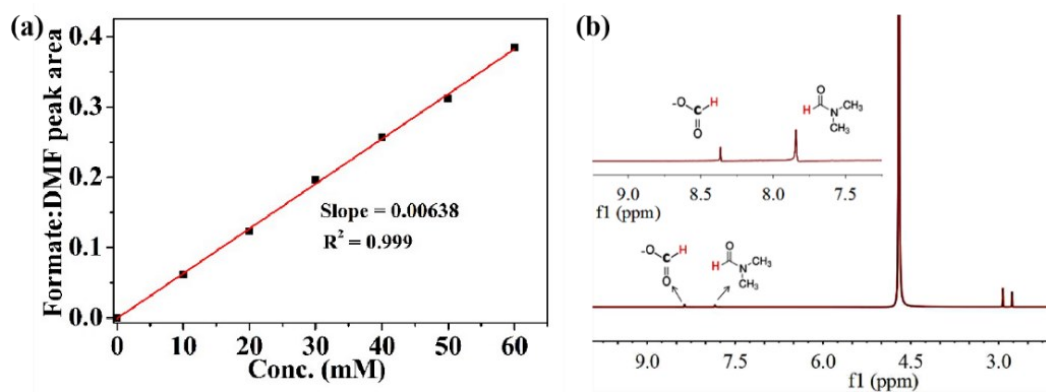
Table S2 The summary table of catalyst performance in the field of CO_2RR.

Electrode Materials	Electrolyte	Potential (V vs. RHE)	$FE_{formate}$ (%)	References
SnO_2-V_O@N-C	0.1 M $KHCO_3$	-1.15	83.8	This work
SnO_2-V_O	0.1 M $KHCO_3$	-1.15	67.8	This work
SnO_2	0.1 M $KHCO_3$	-1.25	58.3	This work
Surface-engineered Sn foil	0.1 M $KHCO_3$	-1.09	77.4	*Catal. Sci. Technol.*, 2017, 7, 2542.
Sn dendrite/Sn foil	0.1 M $KHCO_3$	-1.36	71.6	*ChemSusChem*, 2015, 8, 3092.
Sn quantum sheets confined in graphene	0.1 M $KHCO_3$	-1.26	89	*Nat. Commun.* 2016, 7, 12697.
SnO_2/carbon black	0.1 M $KHCO_3$	-1.26	86.2	*J. Am. Chem. Soc.* 2014, 136, 1734-1737.
Sn(S)/Au needle	0.1 M $KHCO_3$	-0.75	95	*Joule*, 2017, 1, 794.
SnO_2 GDE	0.1 M $KHCO_3$	-1.27	68	*ECS Trans.* 2015, 66, 53-59.
Sn foil	0.1 M $KHCO_3$	-0.95	69.5	*Int. J. Hydrogen Energ.* 2014, 39, 16506-16512.
Sn/SnO_2/Ti	0.1 M $KHCO_3$	-0.70	40	*J. Am. Chem. Soc.* 2012, 134, 1986-1989.

Figure S14 (a) The FE for HCOOH of SnO_2-V_O@N-C in the five-cycle testing. (b) The long-term stability performance of SnO_2-V_O@N-C conducted in the potential of -1.15 V.
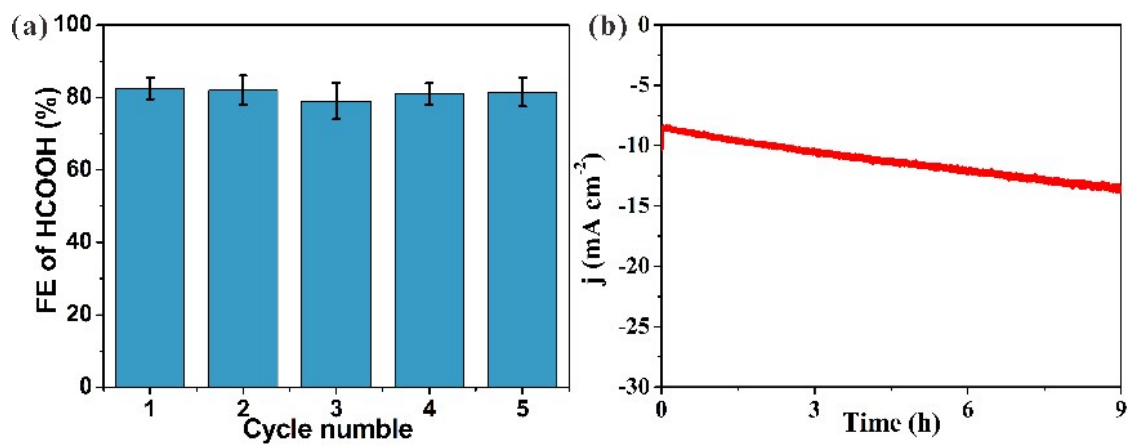
Figure S15 (a) The typical SEM image, (b) TEM image, and (c) the HRTEM image of SnO$_2$-V$_O$@N-C after electrocatalytic process. (d) The high-resolution Sn 3d spectra of SnO$_2$-V$_O$@N-C before and after the electrocatalytic process. (e) The high-resolution O 1s spectrum of SnO$_2$-V$_O$@N-C after the electrocatalytic process. (f) The high-resolution C 1s spectrum of SnO$_2$-V$_O$@N-C after the electrocatalytic process.
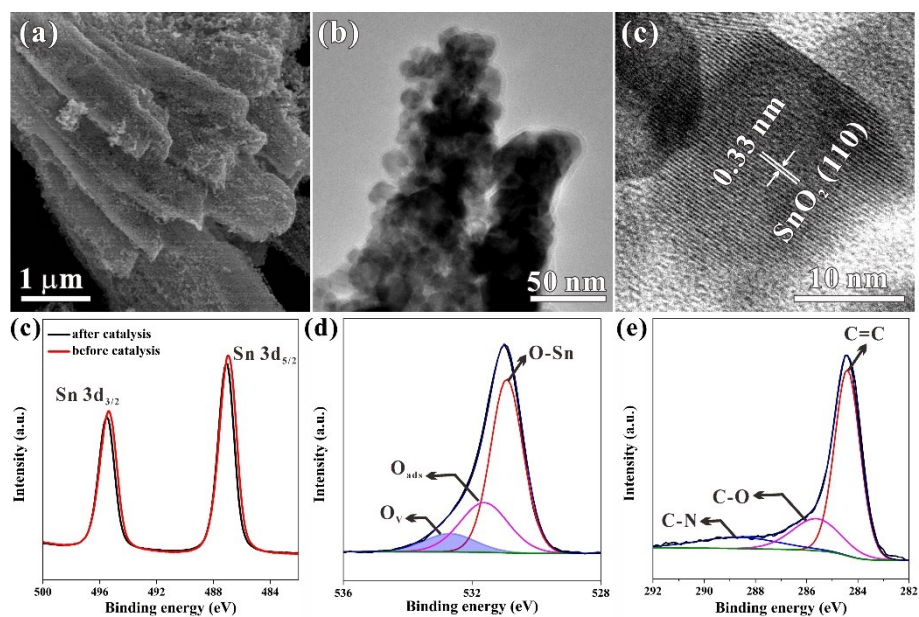
Figure S16 The comparison in the TON for the CO$_2$RR to HCOOH over the three samples.
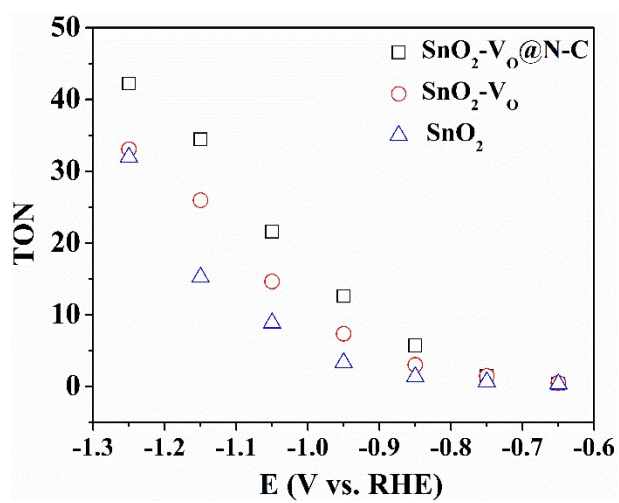
Figure S17 The FE for H_2 over the three electrocatalysts.
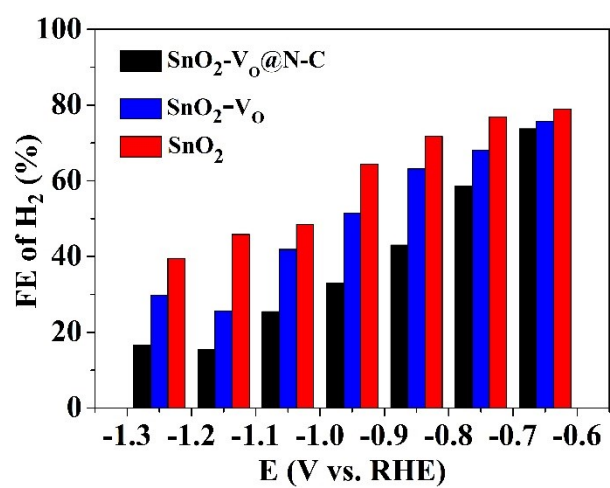
Figure S18 Cyclic voltammograms recorded in the non-faradaic capacitance current range at increasing scan rates: (a) SnO$_2$-V$_O$@N-C, (b) SnO$_2$-V$_O$, (c) SnO$_2$.
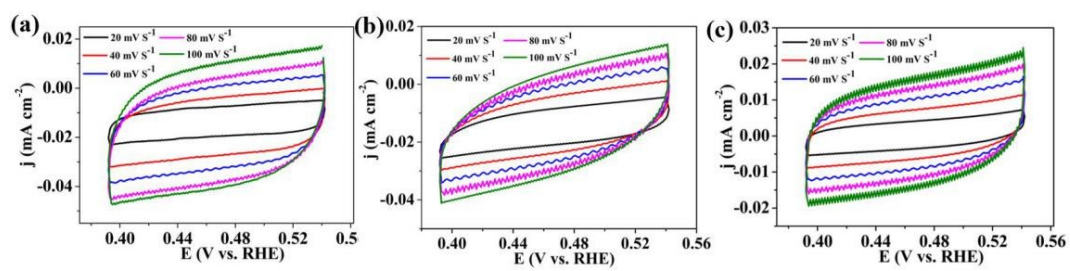
Figure S19 Partial current density for HCOOH corrected by ECSA over the three samples as electrocatalysts.
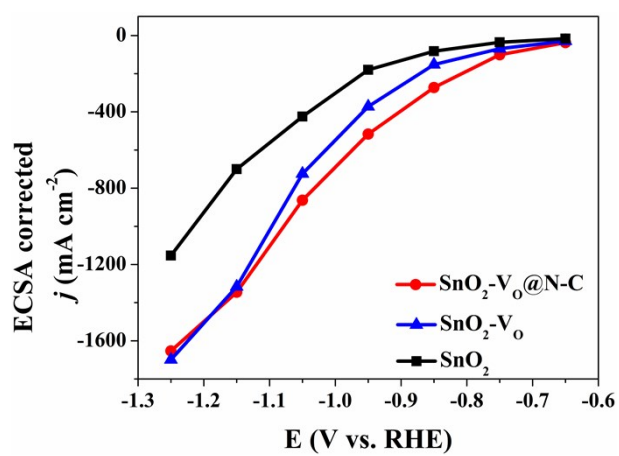
Table S3 The fitting parameters of $SnO_2-V_O@N-C$, SnO_2-V_O and SnO_2.

Sample	R1 (Rs)	R2 (Rct)
$SnO_2-V_O@N-C$	6.78	17.55
SnO_2-V_O	7.09	19.85
SnO_2	6.91	21.65

Figure S20 The Optimized structures of (a) SnO$_2$ (101); (b) N-C; (c) SnO$_2$@N-C; (d) SnO$_2$-Vo@N-C. The O vacancy was generated by missing the circled O in (c).
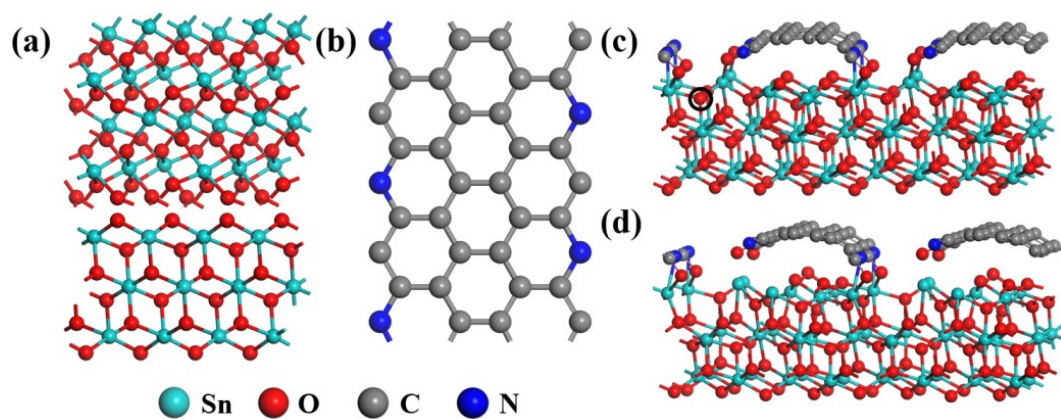
Figure S21 (a) The adsorption configuration of CO_2 of $SnO_2@N$-C. (b) The partial density of states of CO_2 gas adsorbed on $SnO_2@N$-C.
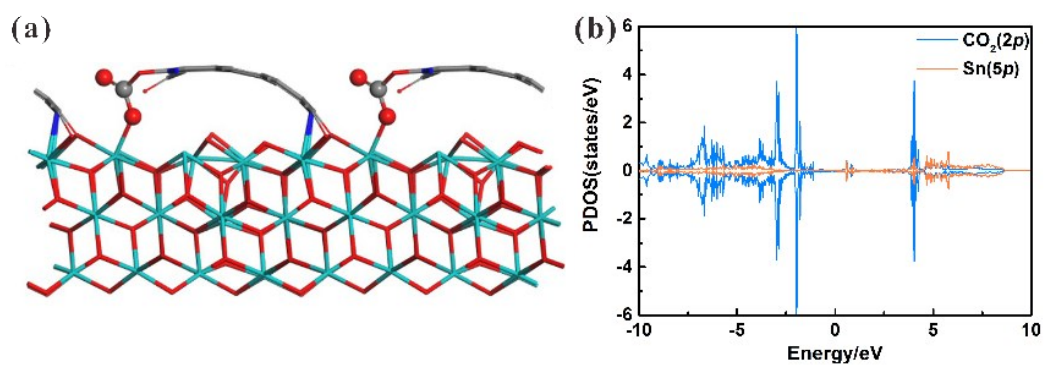
Reference:

[1] G. Kresse, J. F. l., Efficient iterative schemes for ab initio total-energy calculations using a plane-wave basis set. Phys. Rev. B. 1996, 54, 11169-11186.

[2] J. P. Perdew, K. B., Matthias Ernzerhof, Generalized Gradient Approximation Made Simple. Phys. Rev. Lett. 1996, 77, 3865-3868.

[3] G. Kresse, D. J., From ultrasoft pseudopotentials to the projector augmented-wave method. Phys. Rev. B. 1999, 59, 1758-1775.

[4] Grimme, S.; Antony, J.; Ehrlich, S.; Krieg, H., A consistent and accurate ab initio parametrization of density functional dispersion correction (DFT-D) for the 94 elements H-Pu. J. Chem. Phys. 2010, 132, 154104.

[5] J. K. Nørskov, J. R., A. Logadottir, and L. Lindqvist, Origin of the Overpotential for Oxygen Reduction at a Fuel-Cell Cathode. J. Phys. Chem. B. 2004, 108, 17886-17892.